Numerical Studies of Gas Production From Several CH$_4$-Hydrate Zones at the Mallik Site, Mackenzie Delta, Canada

George J. Moridis
Earth Sciences Division, Lawrence Berkeley National Laboratory,
University of California, Berkeley, CA 94720, USA

Timothy S. Collett
United States Geological Survey, Denver, CO 80225-0046, USA

Scott R. Dallimore
Geological Survey of Canada, Sidney, British Columbia V8L 4B2, Canada

Tohru Satoh
Japan National Oil Corporation, Chiba 261-0025, Japan

Steven Hancock and Brian Weatherill
Adams Pearson Associates Inc., Calgary, Alberta T2P 3T6, Canada

May 2002

Abstract

The Mallik site represents an onshore permafrost-associated gas hydrate accumulation in the Mackenzie Delta, Northwest Territories, Canada. A gas hydrate research well was drilled at the site in 1998. The objective of this study is the analysis of various gas production scenarios from several gas-hydrate-bearing zones at the Mallik site. The TOUGH2 general-purpose simulator with the EOSHYDR2 module were used for the analysis. EOSHYDR2 is designed to model the non-isothermal CH_4 release, phase behavior and flow under conditions typical of methane-hydrate deposits by solving the coupled equations of mass and heat balance, and can describe any combination of gas hydrate dissociation mechanisms. Numerical simulations indicated that significant gas hydrate production at the Mallik site was possible by drawing down the pressure on a thin free-gas zone at the base of the hydrate stability field. Gas hydrate zones with underlying aquifers yielded significant gas production entirely from dissociated gas hydrate, but large amounts of produced water. Lithologically isolated gas-hydrate-bearing reservoirs with no underlying free gas or water zones, and gas-hydrate saturations of at least 50% were also studied. In these cases, it was assumed that thermal stimulation by circulating hot water in the well was the method used to induce dissociation. Sensitivity studies indicated that the methane release from the hydrate accumulations increases with gas-hydrate saturation, the initial formation temperature, the temperature of the circulating water in the well, and the formation thermal conductivity. Methane production appears to be less sensitive to the rock and hydrate specific heat and permeability of the formation.

Keywords: gas hydrates; hydrate dissociation; depressurization; thermal stimulation; numerical modeling

1. Introduction

1.1. Background

Gas hydrates are crystalline substances composed of water and gas, in which a solid water-

lattice accommodates gas molecules in a cage-like structure, or clathrate. The estimated amount of gas in the hydrate accumulations of the world greatly exceeds the volume of known conventional gas resources (Sloan, 1998). However, the role that gas hydrates may play in contributing to the world's energy requirements will depend ultimately on the availability of producible gas hydrate resources and the cost to extract them.

The Mallik gas hydrate field, located at the northeastern edge of Canada's Mackenzie Delta, occurs within a sequence of Tertiary sediments in an area underlain by over 600 m of permafrost. With data available from the original Mallik discovery well in 1971 and 1972, and a scientific research well program in 1998, gas hydrate occurrences have been well documented (Dallimore et al., 1999). Quantitative well log determinations and core studies reveal at least 10 discrete gas hydrate layers from -890 m to -1106 m depth, exceeding 110 m in total thickness. High gas hydrate saturation values, which in some cases exceed 80% of the pore volume, establish the Mallik gas hydrate field as one of the most concentrated gas hydrate reservoirs in the world. Thus, Mallik represents an ideal site to test various production schemes for gas hydrate. In this paper, we analyze various gas production scenarios for several gas-hydrate-bearing stratigraphic zones at the Mallik site.

1.2. The numerical model

The analysis of the production scenarios in this paper were conducted using the TOUGH2 general-purpose simulator (Pruess et al., 1999) for multi-component, multiphase fluid and heat flow and transport in the subsurface with the EOSHYDR2 module (Moridis et al., 1998; Moridis, 2002). By solving the coupled equations of mass and heat balance, EOSHYDR2 can model the non-isothermal hydrate formation or dissociation, gas release, phase behavior and flow of fluids and heat under conditions typical of common natural hydrate deposits (i.e., in the permafrost and in deep ocean sediments) in complex formations. The binary hydrate systems that can be studied by EOSHYDR involve methane and a second hydrate-forming gaseous compound G, and their formation and dissociation are described by the general reaction equation

$$\chi_m \left[CH_4 \cdot N_m \, H_2O \right] \cdot \chi_G \left[G \cdot N_G \, H_2O \right] = \chi_m \, CH_4 + \chi_G \, G + (N_m + N_G) H_2O$$
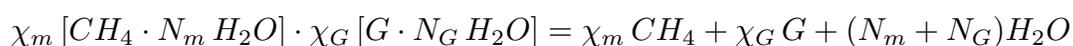
where χ is the mole fraction in the binary hydrate, N is the hydration number, G is the second gas, and the subscripts m and G denote the methane and the second gas, respectively. The second gas G can be another hydrocarbon $C_\nu H_{2\nu+2}$ ($\nu = 2, 3, 4$), or $G \equiv CO_2$, H_2S, or N_2. It is obvious that $\chi_m + \chi_G = 1$. Depending on the prevailing conditions, CH_4 and G are gases during dissociation, but H_2O can be either liquid water or ice.

EOSHYDR2 includes both equilibrium and a kinetic model of gas hydrate formation and dissociation. The model accounts for up to nine components (hydrate, water, native methane and methane from hydrate dissociation, the second native and dissociated gas, salt, water-soluble inhibitors and a heat pseudo-component). The mass components are distributed among four phases, i.e., a gas phase, a liquid phase, and two solid immobile phases: an ice phase and the hydrate phase. The thermophysical properties of the various mass components can be described at temperatures as low as –110 ^{o}C. Dissociation, phase changes and the corresponding thermal effects are fully described, as are the effects of salt and hydrate inhibitors. The model can describe gas hydrate dissociation involving any combination of the possible dissociation mechanisms (i.e., depressurization, thermal stimulation, and salting-out effects).

2. Site geology and simulation zones

2.1. Geological system

The JAPEX/JNOC/GSC Mallik 2L-38 gas hydrate research well, drilled in 1998, was designed to investigate the occurrence of in-situ natural gas hydrates in the Mallik area of the Mackenzie River Delta of Canada (Dallimore et al., 1999). The Mallik 2L-38 gas hydrate research well was drilled near the site of the existing Mallik L-38 well, which was drilled by Imperial Oil in 1972. The Mallik L-38 well is believed to have encountered at least 10 significant gas-hydrate-bearing stratigraphic units within the depth interval from -810.1 to $-1,102.3$ m.

While drilling the Mallik 2L-38 well, a major emphasis was placed on coring the log-inferred gas hydrate intervals identified in the Mallik L-38 well. Approximately 37 m of core was recovered from the gas hydrate interval (from -878 to -944 m) in the Mallik 2L-38 well (Dallimore et al.,

1999). Pore-space gas hydrate and several forms of visible gas hydrate were observed in a variety of sediment types. Analysis of recovered cores and downhole log data from the Mallik 2L-38 well has confirmed the occurrence of gas hydrate within the depth interval from -888.84 m to $-1,101.09$ m; however, not all of this interval contains gas hydrate. The presence of free-gas in contact with gas hydrate occurrences is an important consideration in terms of designing possible production scenarios. It was determined that the Mallik 2L-38 well encountered a relatively thin free-gas zone at the base of the deepest downhole log-inferred gas hydrate accumulation.

The Mallik gas hydrate field, as described by Dallimore et al. (1999), is restricted to the crest of a large anticlinal feature which was penetrated by the Mallik 2L-38 gas hydrate research well. Dallimore et al. (1999) estimated that the Mallik gas hydrate accumulation may hold about 1.1×10^{11} m^3 of gas at standard pressure and temperature conditions.

2.2. *General simulation parameters and conditions*

A total of five zones were investigated. The regional plunge along the crest of the Mallik structure was not considered in the simulations because of the very shallow dip angle (2 degrees to the northwest) and the limited extent of the affected hydrate accumulations during the dissociation process. In all the zones the porosity ($\phi = 0.28$), the intrinsic permeability ($k = 2 \times 10^{-14}$ m^2), the thermal conductivity ($k_\theta = 1.5$ W/m/^{o}C), the rock specific heat ($C_R = 800$ J/kg/^{o}C), and the hydrate specific heat ($C_H = 1600$ J/kg/^{o}C) were assumed to be the same. Note that, even when no-flow boundaries were involved, the simulation domains were appropriately extended to adequately describe the thermal fluxes.

In all simulations, (a) a gas hydrate equilibrium dissociation process was assumed, (b) a hydrostatic pressure distribution was assumed, (c) a heat flux corresponding to the geothermal gradient of $dT/dz = 0.03$ ^{o}C/m was applied to the bottom of the simulated domain, and (d) the gas hydrate was assumed to be a simple methane-hydrate, i.e., $\chi_m = 1$, and the native gas, where present, was 100% methane. Relative permeabilities and capillary pressures were computed from the Parker et al. (1987) three-phase model, in which the immobile hydrate was the third 'organic'

phase. The irreducible water and gas saturations of the Parker et al. (1987) model were $S_{wr} = 0.2$ and $S_{gr} = 0.05$, respectively, and were assumed to be the same in all zones.

3.   The Simulation Zones

3.1.   *Hydrate Zone #1*

3.1.1.   *Properties and characteristics in Zone #1*

Zone #1 is characterized by a 20-m-thick hydrate accumulation, the base of which (at a depth of -1100 m) marks the bottom of the hydrate stability zone. The initial formation temperature at the bottom of the hydrate layer is $T = 13.4^oC$, i.e., the gas hydrate equilibrium temperature at the formation pressure of $P = 10.8$ MPa. The gas hydrate interval has a hydrate saturation $S_H = 0.8$, the rest being water (i.e., $S_w = 0.2$).

In the simulation this interval is capped by a water-saturated siltstone/mudstone sequence that acts as a no-flow boundary, and is underlain by a thin (1.4-m-thick) layer in which gas and liquid water (a brine) coexist. The water and gas saturations in the two-phase zone are shown in Figure 1. It was assumed, that the two-phase zone is underlain by a 15-m-thick water-saturated sandstone unit bounded at the bottom by a tight (no-flow) unit. Zone #1 and its boundaries extend uniformly over a large area. Since hydrates at the bottom of this zone occur at the gas hydrate stability zone, relatively small pressure and/or temperature changes can cause gas hydrate formation or dissociation. Additionally, gas production from the thin two-phase (gas and brine) layer effects depressurization over a relatively large area in contact with the practically impermeable overlying gas hydrates. This, in turn, can induce gas production through gas hydrate dissociation.

3.1.2.   *Production approach and numerical system in Zone #1*

In this study we considered only depressurization of the hydrate interval through a single vertical well completed in the entire two-phase interval. The cylindrical 2-D semi-infinite reservoir domain in this set of simulations was discretized into 57 and 65 non-uniform gridblocks in r and z, respectively, for a total of 3705 gridblocks, of which 3584 were active (the rest being

boundary gridblocks). To capture the dissociation profile in detail and avoid numerical artifacts in the production curves, a very fine discretization scheme was employed in the vicinity of the well, (i.e., $\Delta r = 0.02$ m and $\Delta z = 0.05$ m), but the grid became progressively coarser away from the well. Five mass components (hydrate, water, native methane, methane originating from gas hydrate dissociation, and salt) and heat were described in the simulations, resulting in system of 21504 simultaneous equations. Accounting for the salt is important in this zone because previous studies had shown that salinity at the site was sufficiently large to reduce the hydration temperature at the prevailing pressure by 1.4 ^oC. Given the thermal inertia of the system, such a decrease in the hydration temperature can have a very significant effect on the volume of the produced gas, thus the dilution of the salt in the native water by the water released during dissociation could not be ignored.

To obtain an accurate estimate of the contribution of dissociated gas to the total gas production, the native methane was considered separately from the hydrate-released methane (hereafter referred to as 'dissociated methane'). Fluids were produced from the well at a cumulative rate of $Q = 1.67 \times 10^{-3}$ kg/s, determined through trial-and-error to allow gas production without water flooding for a period of at least 30 days. Brine and gas (mostly methane with minor water vapor) were distributed in the production stream according to their mobilities in the vicinity of the well.

To quantify the effects of the dissociating gas hydrates, two sets of simulations were conducted. In the first set, the gas hydrate layer was assumed to be inert (i.e., non-dissociating), while hydrate dissociation was accounted for in the second set. This approach was implemented to determine whether the two systems had a markedly different response.

3.1.3. *Production from a single vertical well*

The evolution of pressure and temperature at the production interval midpont for the two simulation sets are shown in Figure 2. Note that pressure and temperature are generally uniform and do not exhibit significant vertical variation because of the limited thickness of this interval. Simulations suggest the pressure in the two-phase interval underlaying Zone 1 is significantly higher when gas hydrate dissociation is considered. This is consistent with expectations because of the

contribution of the dissociated methane to the total pressure.

The differences in the temperature response are interesting. For non-dissociating gas hydrates, the temperature rises very slowly (practically imperceptibly) initially, and is then followed by a rapid and monotonic temperature increase as warmer water from deeper in the aquifer is drawn to the well. For dissociating gas hydrates, a temperature drop is first observed. This is consistent with gas hydrate dissociation because of the strongly endothermic nature of this reaction. However, the temperature begins to increase after the initial drop as deeper warmer water moves to the well.

Figure 3 shows F, the mass fraction of gas in the production stream . By maintaining a low total mass production rate, only gas is produced for about 6 days (indicated by a $F \simeq 1$), at which time it begins to decline because of increasing water production. Note that maintaining high gas production is challenging in Zone #1 because of (a) the limited thickness of the two-phase zone, (b) the proximity to the underlying infinite aquifer, (c) the large amounts of water released in the course of gas hydrate dissociation, and (d) an adverse gas relative permeability in the presence of so much native and released water. Note that the effect of released water during dissociation is reflected in the F (compared to that for no dissociation) in the produced stream near the end of the 100-day production period.

The contribution of dissociated methane f to the produced gas (Figure 4) shows that it rises from zero to about 0.45 in about 60 days, after which time it rises very slowly. This indicates that gas hydrate dissociation is a significant source of gas, contributing about half of the produced gas in this geologic scenario and under the production parameters discussed here.

3.1.4. Production from a single horizontal well

We investigated gas production and the corresponding hydrate dissociation (through depressurization) using a single horizontal well. In this case, the center axis of the horizontal well was 0.25 m below the bottom of the hydrate layer in Zone #1, and the perforated interval had a length of 20 m. Fluids were produced from the well at the same rate as in the single vertical well (see Section 3.1.2), resulting in lower pressure drops that were more uniformly distributed along the length of the perforated interval.

Figure 5 shows the evolution of F and f over time in the case of the horizontal well. By distributing the production over the 20 m interval, the pressure changes are significantly lower and result in a delay in the onset of rapid water production from about 6 days to about 9 days. By virtue of its proximity to a larger area of the hydrate interface and the more favorable gas relative permeability regime in the upper part of the two-phase layer (where the horizontal well is located), the contribution of CH_4 from dissociation to the produced gas is larger than that for the vertical well (Figure 4). At the end of the 100-day production period, more than half (52%) of the produced gas originates from methane hydrate dissociation. Although these results tend to indicate that horizontal wells may be more effective means of gas production from hydrates, no definitive conclusion can be reached because, even if economic issues of well construction are ignored, the differences in performance from that in vertical wells is not substantial.

3.1.5. *Production from two-well systems*

The two-well system studied here induced dissociation of the methane hydrates through a combination of depressurization (at the production well) and and thermal stimulation (at the injection well). The distance between the two vertical wells was 50 m. The injection and production intervals were located in the upper 0.5 m of the two-phase layer.

We investigated the injection of two hot fluids. The first was steam with a specific enthalpy of 3200 kJ/kg, i.e., with sufficiently high enthalpy to remain superheated steam at the injection pressure. In this case, the steam injection rate and the fluid production rate were the same, and equal to $Q = 1.67 \times 10^{-3}$ kg/s. Although much higher injection and production rates are possible in such a well configuration, the rates were kept at this low level to allow a meaningful performance comparison to those in the vertical and horizontal single wells. The second hot fluid was methane with a specific enthalpy equal to that of the steam. In this case, CH_4 was injected at a rate of 8.35×10^{-4} kg/s (i.e., half that of the injected steam), while fluids were produced at the production well at a rate of $Q = 2.51 \times 10^{-3}$ kg/s (thus, maintaining an effective production rate of $Q = 1.67 \times 10^{-3}$ kg/s). Note that in this study we did not address potential practical problems, or safety concerns, involved in the heating and injection of CH_4, but concentrated instead on the

study of general strategies that can maximize production.

The cartesian 3-D reservoir grid in this set of simulations involved domain discretization into $76 \times 31 \times 36$ non-uniform gridblocks in x, y, z, for a total of 84816 gridblocks, of which 75480 were active. To accurately capture the dissociation profiles, a very fine discretization was used in the vicinity of the two wells. The simulations solved for the same six components involved in the single well studies (see Section 3.1.2), resulting in a system of 452880 equations.

The review of the evolution of F over time in the two-well system in Figure 6 shows that, when steam is injected, the onset of significant water production is delayed to about 12 days. Additionally, after a rapid initial decline, the rate of decline in F is substantially reduced, and the F at $t = 100$ days is much higher than that for the single vertical or horizontal wells. This despite the fact that the injection of steam inevitably adds water to the system (after condensation), thus adversely affacting the gas relative permeability.

The injection of the hot CH_4 shows even more interesting results. The onset of water production is delayed to about 14 days, but F declines only to about 0.7 at $t = 30$ days, after which time it rises very slowly. The slow rise coincides with the arrival at the production well of the hot gas stream from the injection well. The behavior of F indicates that, despite producing from a very thin two-phase zone underlain by a large aquifer, it is possible to maintain a high F in the production stream. This is attributed to the favorable gas relative permeability regime. The buoyancy of the injected hot CH_4 directs it to the top of the two-phase layer, where it displaces native water while ensuring maximum contact with the hydrate, i.e., the intended target. Thus, aided by the pressure differential between the two wells, a high gas saturation zone is established underneath the hydrate interface. This zones keeps expanding upward as the interface recedes. The fact that the injected CH_4 (unlike the steam) is non-condensible helps reduce adverse relative permeability effects to a minimum, maximizing production and performance in the process.

More encouraging results are provided by Figure 7 that shows the evolution of f in the two-well system. Thus, f rises continuously (though very slowly after $t = 60$ days) to as high as 0.61 in the case of steam injection, and to an even higher level ($f \simeq 0.72$) in the case of hot CH_4

injection. These results indicate that, in two-well configurations (and, by extension, in five-spot arrangements), the majority of the produced gas originates from the dissociation of the methane hydrates. The injection of hot CH_4 appears to have an advantage over steam injection. However, these results should be viewed as indicative rather than definitive because of the preliminary stage of these studies.

3.2. Hydrate Zone #2

3.2.1. Properties and characteristics in Zone #2

Zone #2 is characterized by a 16-m-thick hydrate-bearing interval (from -899 to -915 m, with $S_H = 0.5$, and $T = 7.5\ ^oC$, $P = 9$ MPa at the base of the hydrate interval) capped by a relatively thick gas-hydrate-bearing sandstone sequence with varying gas-hydrate saturations. This gas hydrate accumulation is underlain by a 2-m-thick water-saturated layer, followed by a 2-m-thick low-porosity ($\phi < 0.02$) sandstone that is assumed to act as a flow boundary. Because of its shallower depth, Zone #2 is cooler than Zone #1. Zone #2 and its boundaries are assumed to extend uniformly over a large area.

3.2.2. Production approach and numerical system in Zone #2

As in Zone #1, the only dissociation method we considered was depressurization of the gas hydrate accumulation through fluid withdrawals from the underlying water-saturated zone. The very low compressibility of water was expected to provide conditions conducive to dissociation through depressurization because the pressure decline is transmitted more effectively (compared to a free gas zone) over a larger area of the hydrate interface.

The cylindrical 2-D grid involved 65 and 38 non-uniform gridblocks in r and z, respectively, for a total of 2210 gridblocks. The simulations accounted for heat and four components (hydrate, water, dissociated methane, and salt), resulting in a system of 12350 simultaneous equations. Water was produced from the well (completed in the 2-m water-saturated layer) at a rate of $Q_w = 0.58$ kg/s (a rate than can be sustained without cavitation). The corresponding rate of CH_4 production was computed internally by the model from the aqueous and gas phase mobilities near the wellbore.

3.2.3. Production predictions and analysis in Zone #2

Figure 8 shows the cumulative gas production over time. Note that the gas phase emerges only after about 5 days of continuous water production. There are two reasons for the delay in gas appearance. The first is the adverse relative permeability conditions (emergence of a gas phase in a previously fully-saturated formation, coupled with the release of large amounts of water during dissociation) that necessitate a gas saturation $S_g > 0.05$ for gas mobility. The second reason is the low initial temperature (at the formation pressure of 9 MPa, the dissociation temperature is 11.5 ^{o}C) that requires a larger pressure drop (and, thus, longer fluid withdrawal) to effect dissociation through depressurization. Note that the shape of the cumulative gas production curve indicates a continuously decline gas production rate as the pressure approaches a steady-state distribution (with the boundaries replenishing the withdrawn water) and the gas hydrate reach a new pressure-temperature equilibrium point at a lower temperature (because of the dissociation heat is absorbed by the system in the vicinity of the dissociating hydrate).

An important observation from Figure 8 is that a large volume of gas can be produced from Zone #2, and all of it originates from gas hydrate dissociation. While this is promising, the potential of this single-well approach is limited by the large volume of produced water, which may have negative economic and environmental implications. This is demonstrated by the very low gas mass fraction in the production stream (Figure 9), which does not exceed 0.017 over the simulation period.

3.3. Hydrate Zones #3, #4 and #5

3.3.1. Properties and characteristics in Zones #3 to #5

These three zones are discussed together because they are all characterized by the absence of any underlying layers of mobile gas or water. In these zones, the pore space is occupied by gas hydrate and water (mostly immobile), and the hydrate interval occupies the entire zone thickness.

Zone #3 extends from a depth of about -1081 m to -1091 m, and has a $S_H = 0.8$, and $T = 12.8\,^o$C and $P = 10.74$ MPa, at the base of the hydrate interval. It is the deepest and warmest of these three zones, and, as such, closer to the hydration equilibrium and the easiest to dissociate. Zone #3 is capped by a relatively thick siltstone sequence, and is underlain by a relatively thick

gas-hydrate-bearing sandstone sequence with varying gas-hydrate saturations.

Zone #4 extends from a depth of -1007 m to -1017 m, and is capped and underlain by relatively thick sandstone sequences with varying gas-hydrate saturations. This zone has a lower hydrate saturation ($S_H = 0.5$) and, at the base of the hydrate interval, $T = 10.5\ ^oC$ and $P = 10.0$ MPa. Zone #5 ($S_H = 0.8$ and $P = 8.9$ MPa at the bottom of the hydrate layer) is shallower (from a depth of -905 m to -915 m) and colder ($T = 7.5^oC$) because of its proximity to the permafrost, and its top and bottom boundaries are similar to those of Zone #4.

3.3.2. *Production approach and numerical systems in Zones #3 to #5*

Because of the high S_H in all three zones and the absence of an initial gas phase, the relative permeability to both the aqueous and the gas phases are very small. Coupled with the absence of free gas or water zones underlaying or overlaying the hydrate interval, this creates an adverse permeability environment that severely restricts flow, confines pressure changes to a very small portion of the hydrate deposit, and severely limits (if it does not preclude) the use of a depressurization approach to hydrate dissociation. Note that no hydrate fracturing was considered in this analysis.

Tthe adverse permeability conditions, we focused on thermal stimulation as the mechanism for hydrate dissociation in Zones #3 through #5. The production strategy we investigated involved the circulation of hot water in a single vertical well completed in the gas hydrate interval. The hot water column maintained constant pressure (hydrostatic) and temperature conditions at the well, and the the heat for the hydrate dissociation was provided through conduction and, to a far lesser extent and later in the simulation period, advection.

The same cylindrical 2-D grid was used in the simulations of gas hydrate dissociation in Zones #3, #4 and #5. The hydrate zones were subdivided into 82 and 20 non-uniform gridblocks in (r, z), respectively, for a total of 1640 gridblocks. The simulations accounted for heat and three mass components (hydrate, water, and dissociated methane), resulting in a system of 6560 equations. In all simulations, the wellbore temperature was maintained at $T_w = 50\ ^oC$, and the well was kept at the corresponding hydrostatic pressure.

3.3.3. *Production predictions and analysis*

Figure 10 shows the evolution of pressure at the midpoint of the hydrate interval as Zone #3 is exposed to the hot water. The observed pressure surge exceeds the hydrostatic fluid pressure by a factor of as high as 2.5. The reason for the very high pressure is the sudden release of a large volume of methane from the dissociating gas hydrate (1 m^3 of hydrate releases 164 m^3 of methane under standard conditions) in response to the thermal stimulation, and the ease of dissociation because of the proximity of temperature to the hydration temperature at the prevailing pressure. Under these conditions of limited flow, thermal stimulation is a more effective mechanism than depressurization, a fact confirmed by the gas hydrate equilibrium pressure-temperature relationship indicates (Moridis, 2002). The large methane volume is released into the limited pore space that was previously occupied by only the nearly incompressible water. This, coupled with the extremely low effective permeability of the gas-hydrate-bearing formation (a result of $S_H = 0.8$), which does not allow the gas to move radially away from the well and the pressure to dissipate, causes the pressure spike. The peak pressure decreases over time as the released gas escapes through the well and the dissociation front advances (with a corresponding increase in the permeable pore space).

Figure 11 shows the distribution of temperature over time during the same period. Note the absence of a discernible temperature drop at the leading edge of the advancing temperature front. This indicates that the system thermal conductivity (probably the grain-to-grain contact of the more conductive solid grains) is sufficiently large to provide the needed dissociation heat. Another important observation from Figure 11 is that the reach of the temperature front during the 30-day simulation period is only about 4 m. This is indicative of the position of the dissociation front, although of limited accuracy because of the shifting dissociation temperature (because of the increase in pressure, see Figure 10).

The position of the dissociation fronts in Zones #3, #4 and #5 over time is shown in Figure 12. In Zone #3, the dissociation front at $t = 30$ days is at a radius of only about 3 m, confirming the indications of the temperature profile. The dissociation radius is significantly smaller in Zone #4, and even smaller in the much colder Zone #5.

The cumulative gas production in Zones #3, #4 and #5 is shown in Figure 13. The volume of the dissociated gas from Zone #3 is about 5 times larger than the corresponding volumes from Zone #5. This significant difference is due to the higher temperature that is close to the dissociation temperature at the pressure of Zone #3. Thus, heat addition is used mostly for dissociation, without being consumed to raise the temperature of the hydrate (a relative insulator). This is demonstrated by the gas production from the colder Zone #5, which is smaller by a factor of five than that from Zone #3 despite having the same $S_H = 0.8$. Although the dissociation front advances much further in Zone #4 (Figure 12), the volume of the released gas is about the same as that from Zone #5 because of the lower $S_H = 0.5$.

4. Sensitivity Analysis of Thermal Dissociation

We conducted sensitivity analyses of CH_4 production from thermally-induced dissociation to determine the governing parameters and assess their relative importance. We investigated the effect of S_H, T, k_θ, k, C_H and C_R, as well as the impact of the boundary conditions at the well during tharmal stimulation. In the sensitivity analyses, we considered a single vertical production well, and assumed a uniform distribution of the various parameters of interest.

4.1. Effect of S_H

For a constant temperature T_w of the hot circulating water at the well, a higher S_H is expected to correspond to larger volumes of produced CH_4 because of larger hydrate abundance. The substantial increase in the volume of the released gas when S_H in Zone #4 increases from 0.5 to 0.8 in Figure 14 confirms this expectation. Note, however, that the increase in the released gas volume is sublinear. This is attributed to the larger thermal insulating effect of a larger S_H because of the low conductivity of the hydrate. Thus, a relatively larger portion of the added heat is needed to increase the hydrate temperature to the dissociation point.

4.2. Effect of T and k_θ

Figure 15 compiles the effect of formation temperature and thermal conductivity on gas release

versus time using the gas production form Zone #5 as a baseline. The initial formation temperature T appears to have a dramatic effect on gas production. Thus, a $3.5\,^oC$ temperature difference (between the initial T in Zone #5 and the hydration temperature $T_H = 11\ ^oC$ at the formation pressure), is shown to reduce production by a factor of about four. This behavior is due to the substantial amount of heat needed to raise the temperature of the hydrate (a relative thermal insulator) to the dissociation temperature T_H.

Figure 15 also shows the strong dependence of gas production from dissociating hydrates on the thermal conductivity k_θ. When k_θ decreases from the baseline value of 1.5 W/m/^oC to 1.0 W/m/^oC and 0.5 W/m/^oC, the corresponding reduction in the volume of the produced gas appears to be linear. This conforms with expectations because a decrease in conductivity leads to a linear decline in the rate at which heat is supplied to the dissociating front.

4.3. Effect of the Well Boundary Conditions

When the well temperature T_w increases from $50\ ^oC$ to $70\ ^oC$, the produced gas volume increases by about 25% (Figure 16). The reason for this modest increase is the dependence of the heat flux into the hydrate interval on the temperature differential between the circulating hot water and the formation adjacent to the well. This temperature differential decreases continuusly over time, and the higher well temperature is insufficient to counteract this decline.

The pressure conditions at the well combined with the manner of heat addition appear to have the most dramatic effect on gas production. Thus, heat addition at a constant rate of $Q_H = 6$kW increases gas production by 40% when the wellbore is kept at the hydrostatic pressure of the circulating water (denoted by 'a' in Figure 16). For comparison, the change of Q_H over time at a constant T_w is shown in Figure 17, which indicates that a constant power input at the well alleviates the problem of continuous Q_H decline as the temperature differential at the well decreases. Note that, although about double the heat is added when Q_H is a constant 6kW, the increase in gas production is only 40% because of the large thermal inertia of the system.

When, however, heat is added at a rate of $Q_H = 6$kW) and the well is kept dry at atmospheric pressure (e.g., by artificial lift production of the water released during dissociation), then gas

production increases by about an order of magnitude (denoted by 'b' in Figure 16). This is due to the combined effect of thermal stimulation of the gas hydrate and depressurization (as the hydrate interval is exposed to the atmospheric rather than the hydrostatic pressure).

4.4. Effect of k, C_H and C_R

Figure 18 shows that gas production under the aforementioned conditions appears to be practically insensitive to the formation permeability k when k increased from 2×10^{-14} m^2 (20 mD) to 10^{-13} m^2 (100 mD). This is attributed to the very high pressures that develop after the gas release (see Section 3.3.3) and the very limited radius of the dissociated hydrate zone that the released gas has to cross before reaching the well.

It is noteworthy that gas production appears insensitive to the specific heat of the gas hydrate C_H, and the released volumes barely differ when C_H is reduced from 1600 J/kg/^{o}C to 1300 J/kg/^{o}C (Figure 18). This is probably because, unlike the porous medium, the hydrate has a low density and occupies only a portion of the pore volume, thus it is not the dominant component per unit volume and unit mass of the system. Conversely, the dominance of the porous medium in the mass and heat balance affects gas production. Thus, the volume of released CH$_4$ decreases (albeit mildly) as C_R increases from 800 J/kg/^{o}C to 1000 J/kg/^{o}C (Figure 18). This is consistent with expectations, because a larger C_R indicates more energy stored in the rock per unit temperature and unit mass, with a corresponding reduction in the energy available for hydrate dissociation.

5. Conclusions

The following conclusions can be drawn from the numerical simulation study of gas production from the five zones at the Mallik site:

1. Production from Zone #1 (with a free gas zone underlying the gas hydrate deposit) by depressurization is possible. Single horizontal wells appear to have an advantage over single vertical wells by delaying water upconing and leading to higher contributions of CH$_4$ from dissociation to the production gas stream. Two-well systems involving a combination of

depressurization (at the production well) and thermal stimulation (at the injection well, where hot fluids are injected) appear to be substantially superior to single well systems, and their advantages are more evident if hot non-condensible gases are injected.

2. Depressurization of Zone #2 (a gas hydrate underlain by an aquifer) yields gas but also large amounts of water.

3. In Zones #3 through #5 (gas hydrates with no underlying free-gas or water zones, and a gas-hydrate saturation of at least 50stimulation yields measurable amounts of dissociated gas.

4. Under the conditions of Zones #3 through #5, sensitivity studies indicate that the gas production from the hydrate accumulations increases with the gas-hydrate saturation, the hydrate initial temperature, the temperature of the circulating water in the well, and the thermal conductivity of the system, the method of heat addition, and the pressure at which the well is kept. Gas production appears to be less sensitive to the rock and gas hydrate specific heat and the permeability of the formation.

Acknowledgements

5. REFERENCES

Corey, A.T. (1954). The interrelation between gas and oil relative permeabilities. Producers Monthly, 38-41.

Dallimore, S.R., Uchida, T., and Collett, T.S. (1999), eds.. Scientific Results from the JAPEX/JNOC/GSC Mallik 2L-38 Gas Hydrate Research Well, Mackenzie Delta, Northwest Territories, Canada, Geological Survey of Canada Bulletin 544.

Moridis, G.J., Apps, J., Prues, K., and Myer, L. (1998). EOSHYDR: A TOUGH2 module for CH_4-

hydrate release and flow in the subsurface. Report LBNL-42386, Lawrence Berkeley National Laboratory, Berkeley, CA.

Moridis, G.J. (2002). Numerical simulation of gas production from methane hydrates. SPE 75691, To appear in the Proceedings, SPE 2002 Gas Technology Symposium, Calgary, Alberta, Canada, April 30-May 2, 2002.

Parker, J.C., Lenhard, R.J., and Kuppusamy, T. (1987). A parametric model for constitutive properties governing multiphase flow in porous media. Water Resour. Res. 23(4), 618-624.

Pruess, K., Oldenburg, C., and Moridis, G. (1999). TOUGH2 Users Guide – Version 2.0. Report LBL-43134, Lawrence Berkeley national Laboratory, Berkeley, CA.

Sloan, E.D. (1998) Clathrate Hydrates of Natural Gases, Marcel Dekker, Inc., New York, NY.
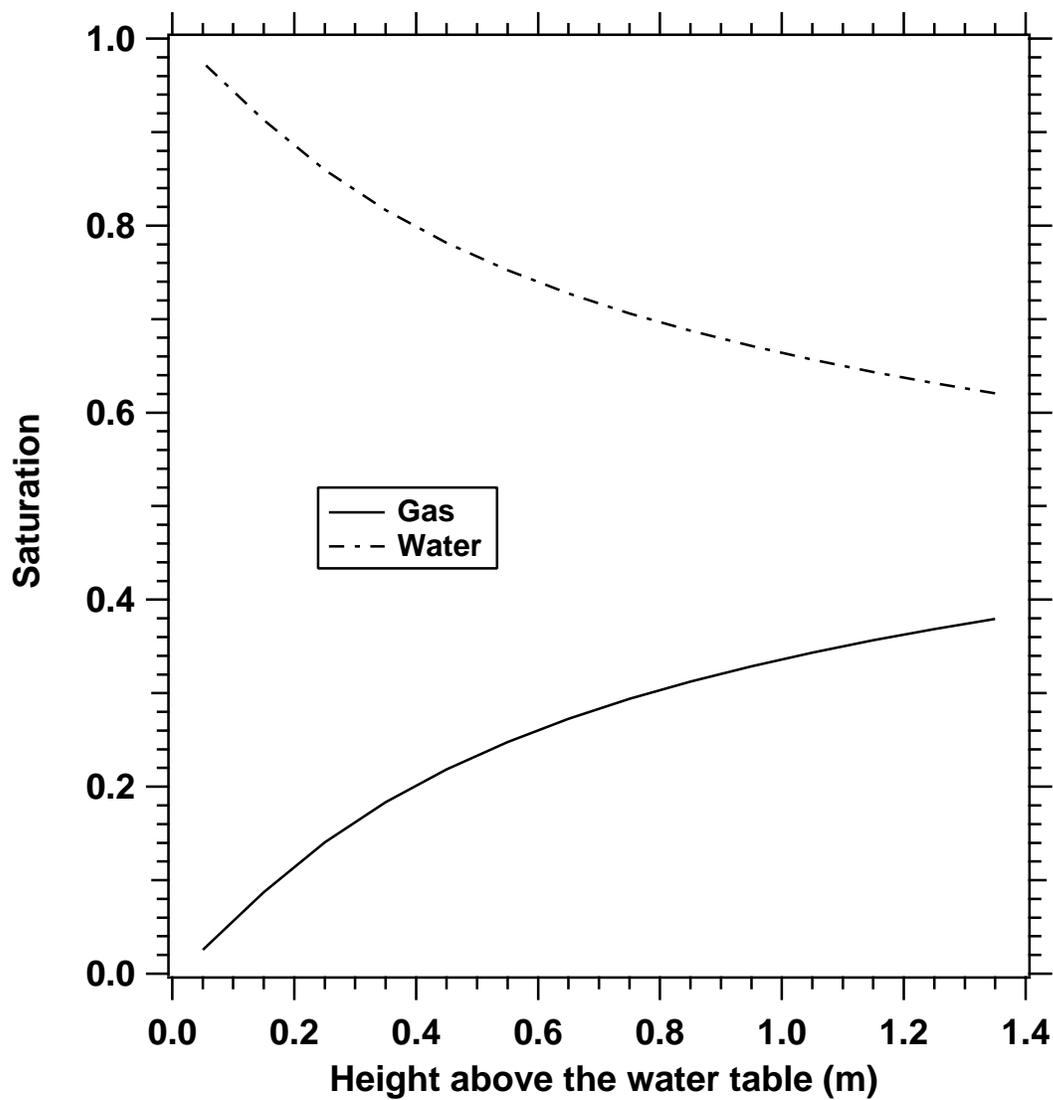
Fig. 1. Water and gas saturation in the two-phase layer in Zone #1.
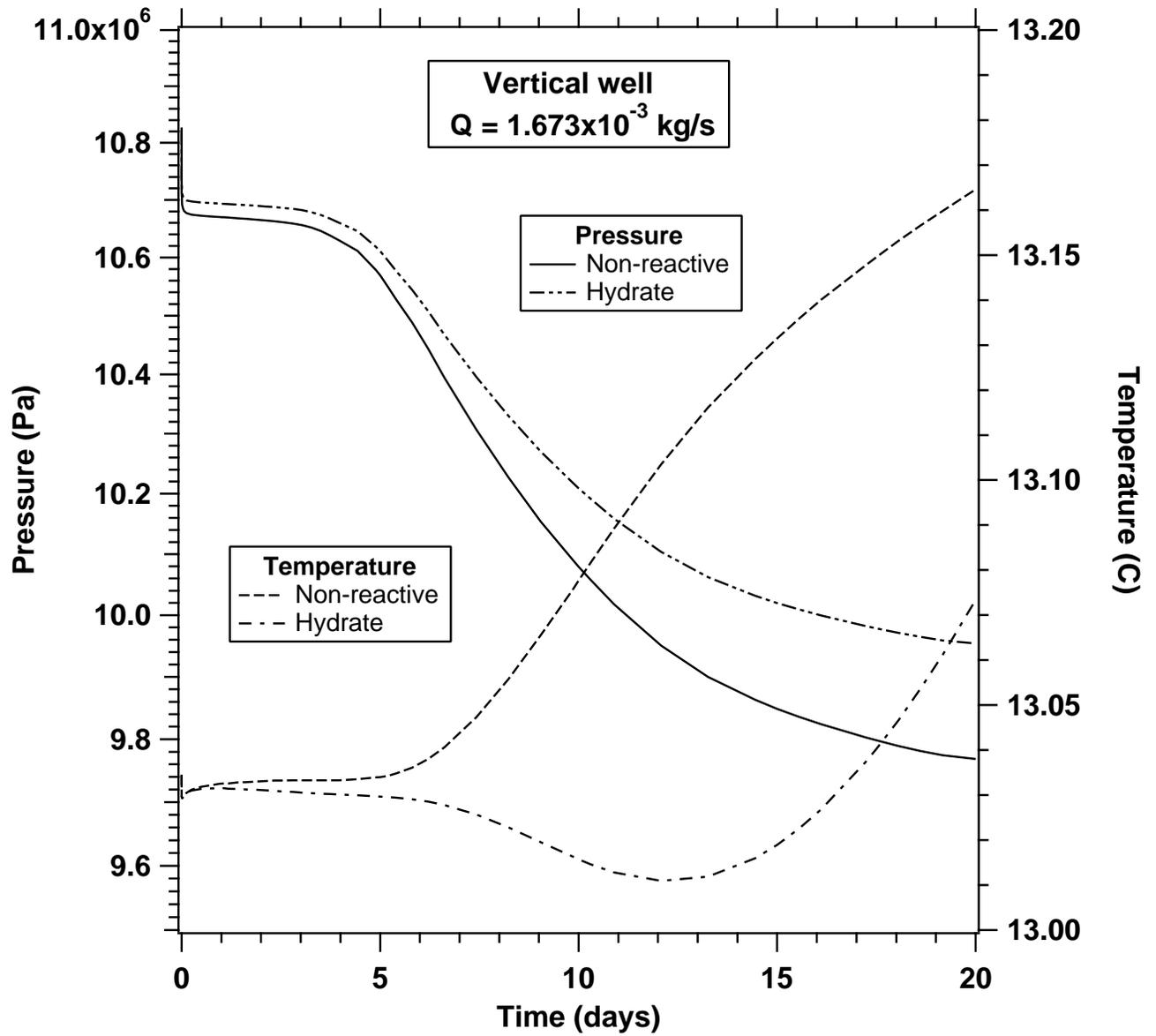
Fig. 2. Evolution of pressure and temperature at the vertical well in Zone #1.
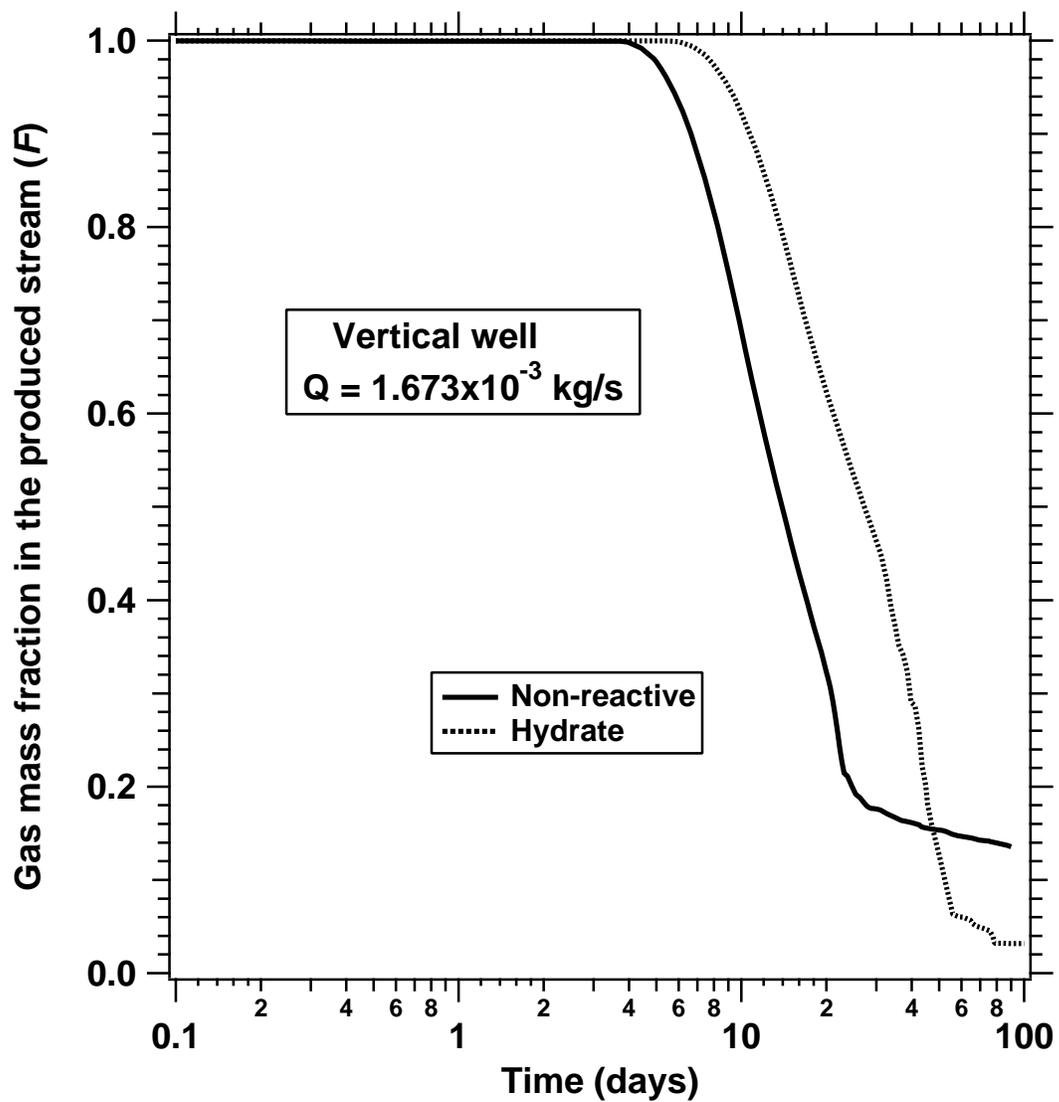
Fig. 3. Gas mass fraction in the production stream of the vertical well in Zone #1.
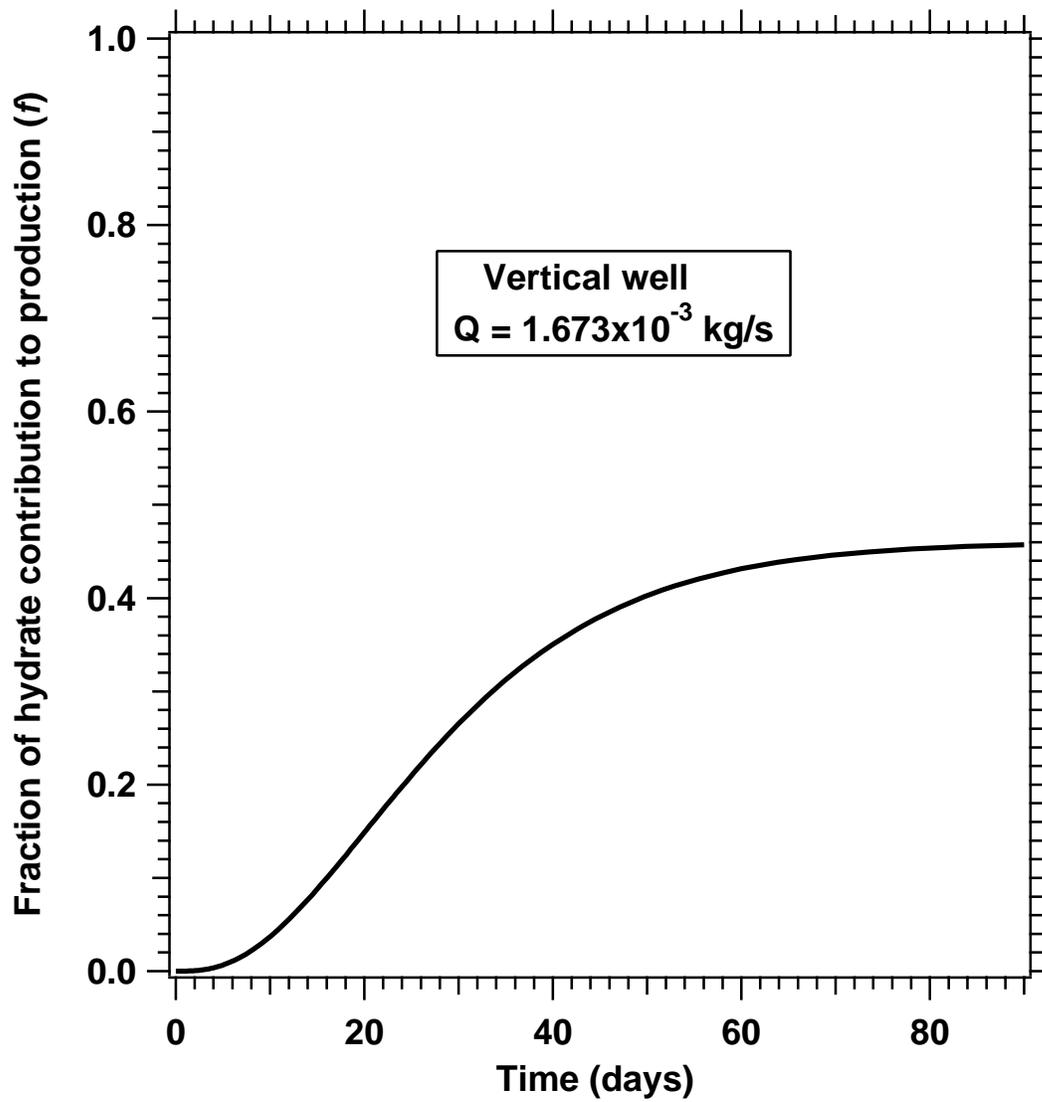
Fig. 4. Hydrate contribution to gas production stream in Zone #1 (vertical well).
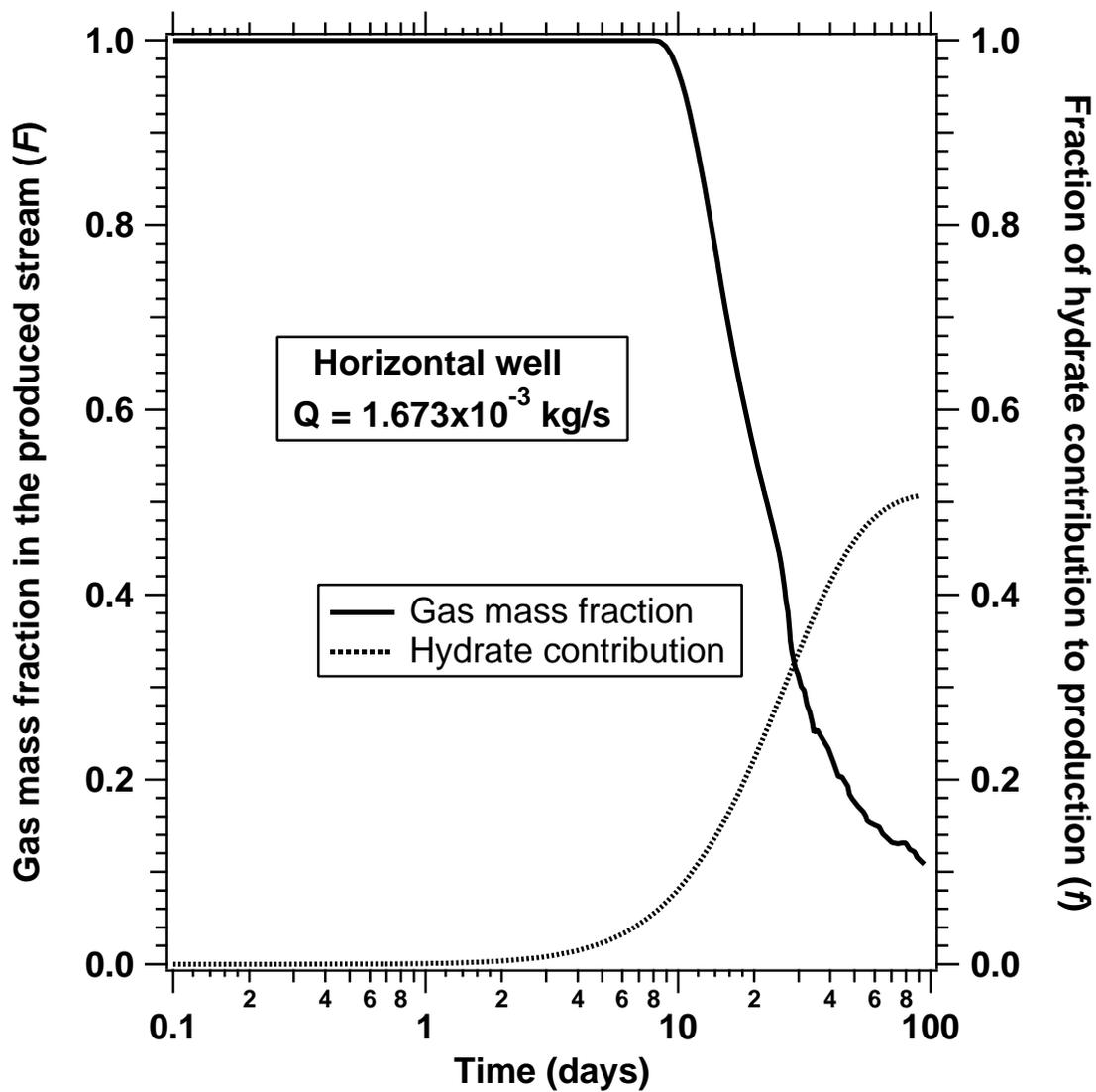
Fig. 5. Gas mass fraction in the production stream and hydrate contribution to gas production stream in Zone #1 (horizontal well).
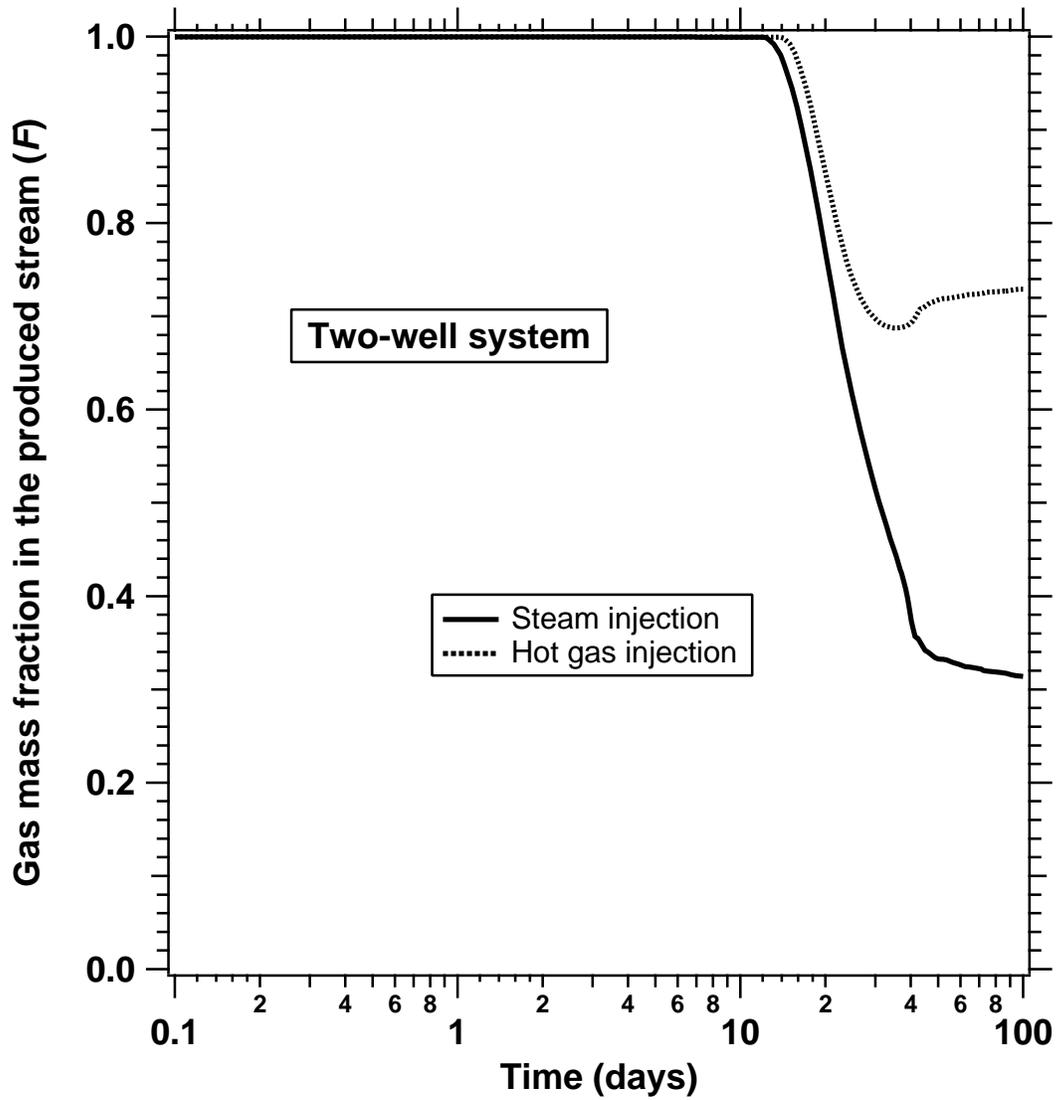
Fig. 6. Gas mass fraction in the production stream of the two-well system in Zone #1.
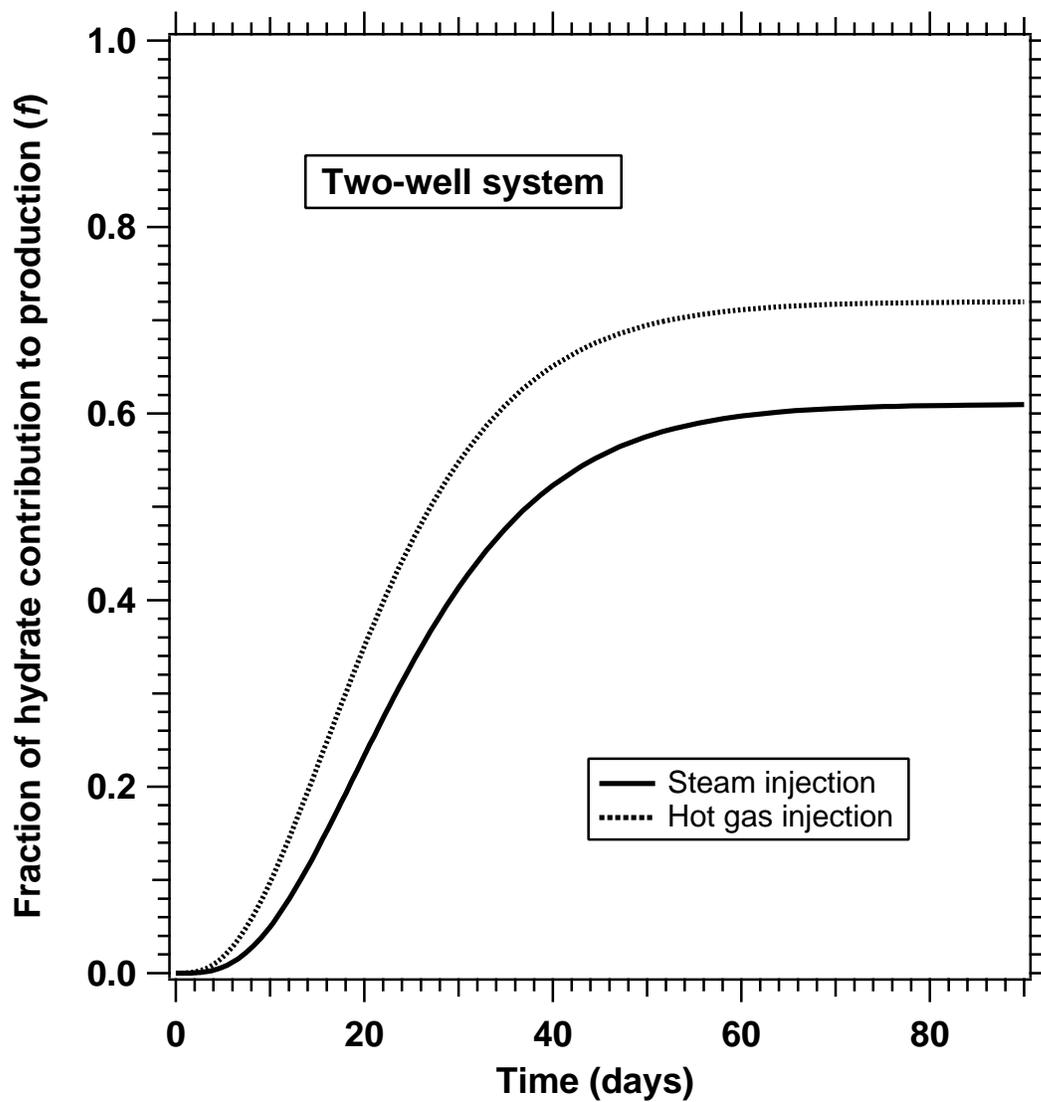
Fig. 7. Hydrate contribution to gas production stream of the two-well system in Zone #1.
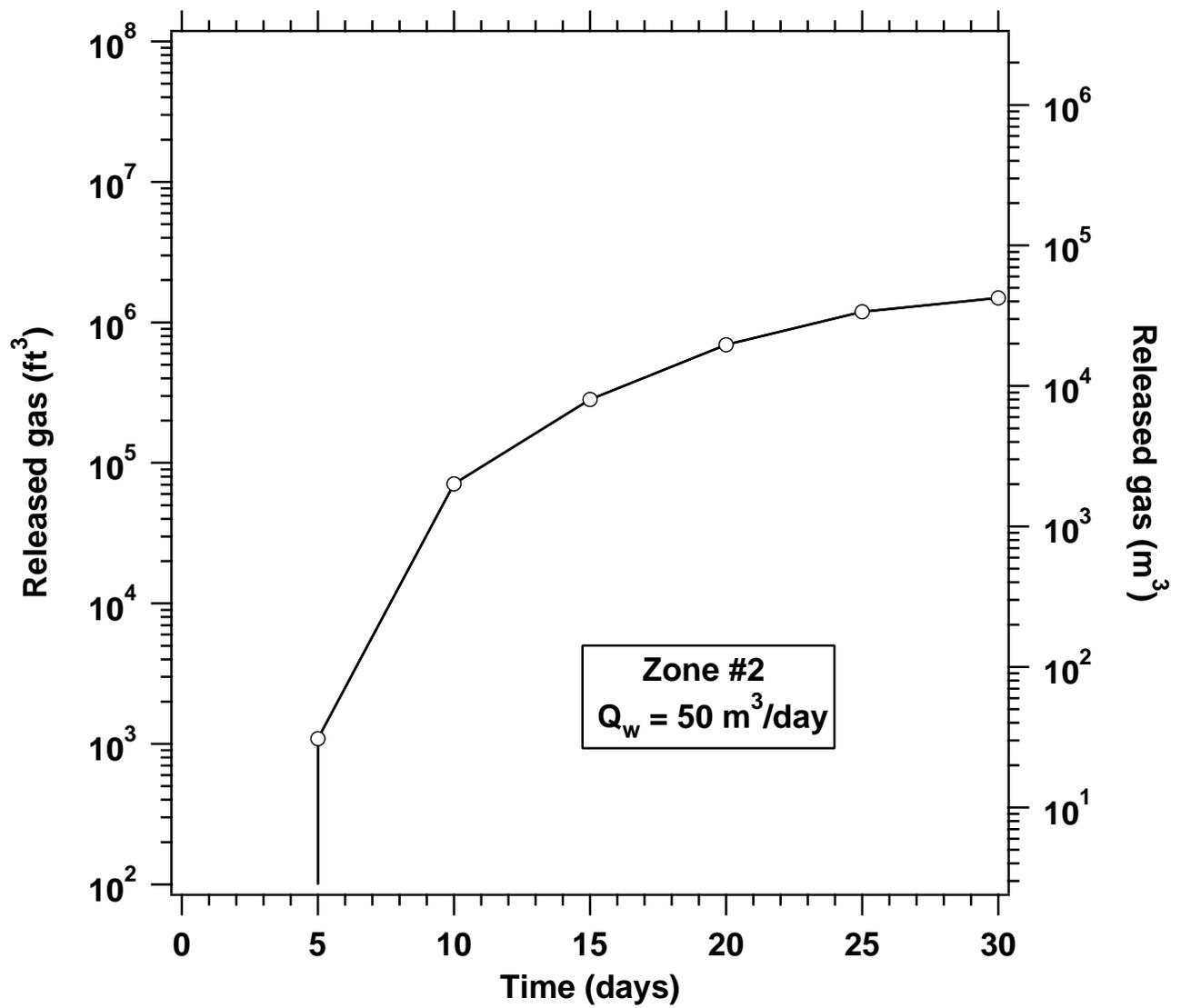
Fig. 8. Cumulative gas production in Zone #2.
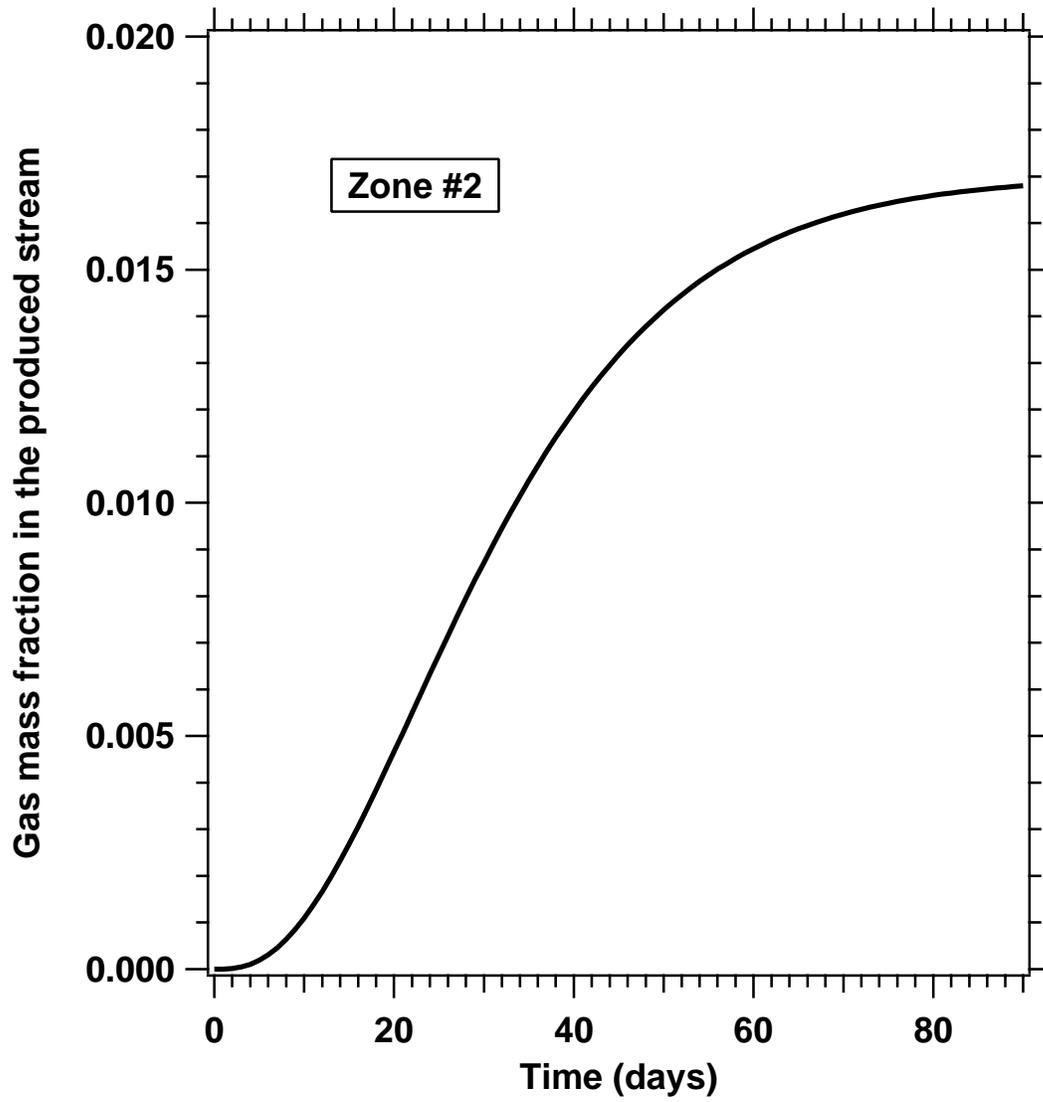
Fig. 9. Gas mass fraction F in the production stream of Zone #2.
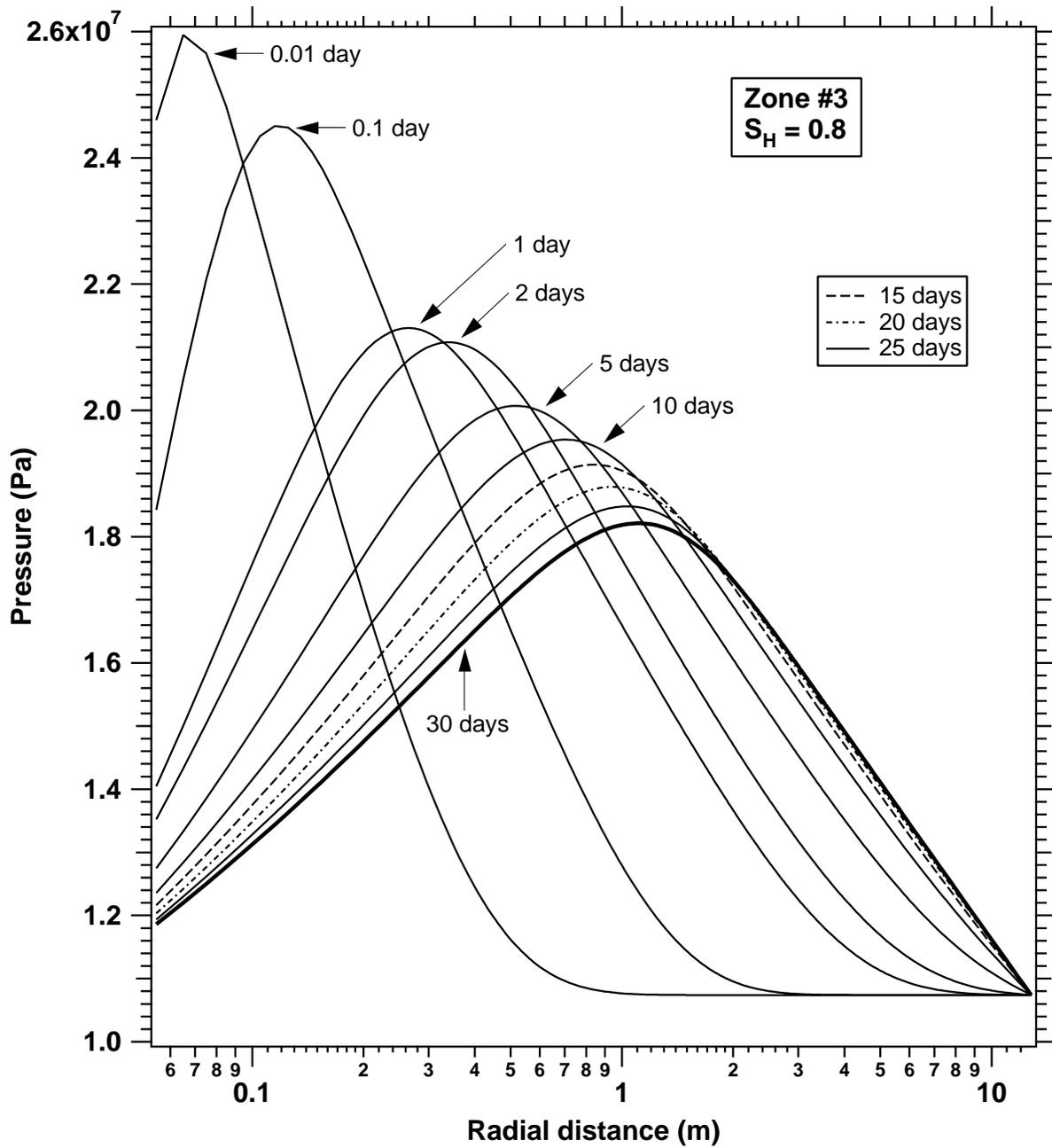
Fig. 10. Formation pressure during thermal dissociation of hydrates in Zone #3.
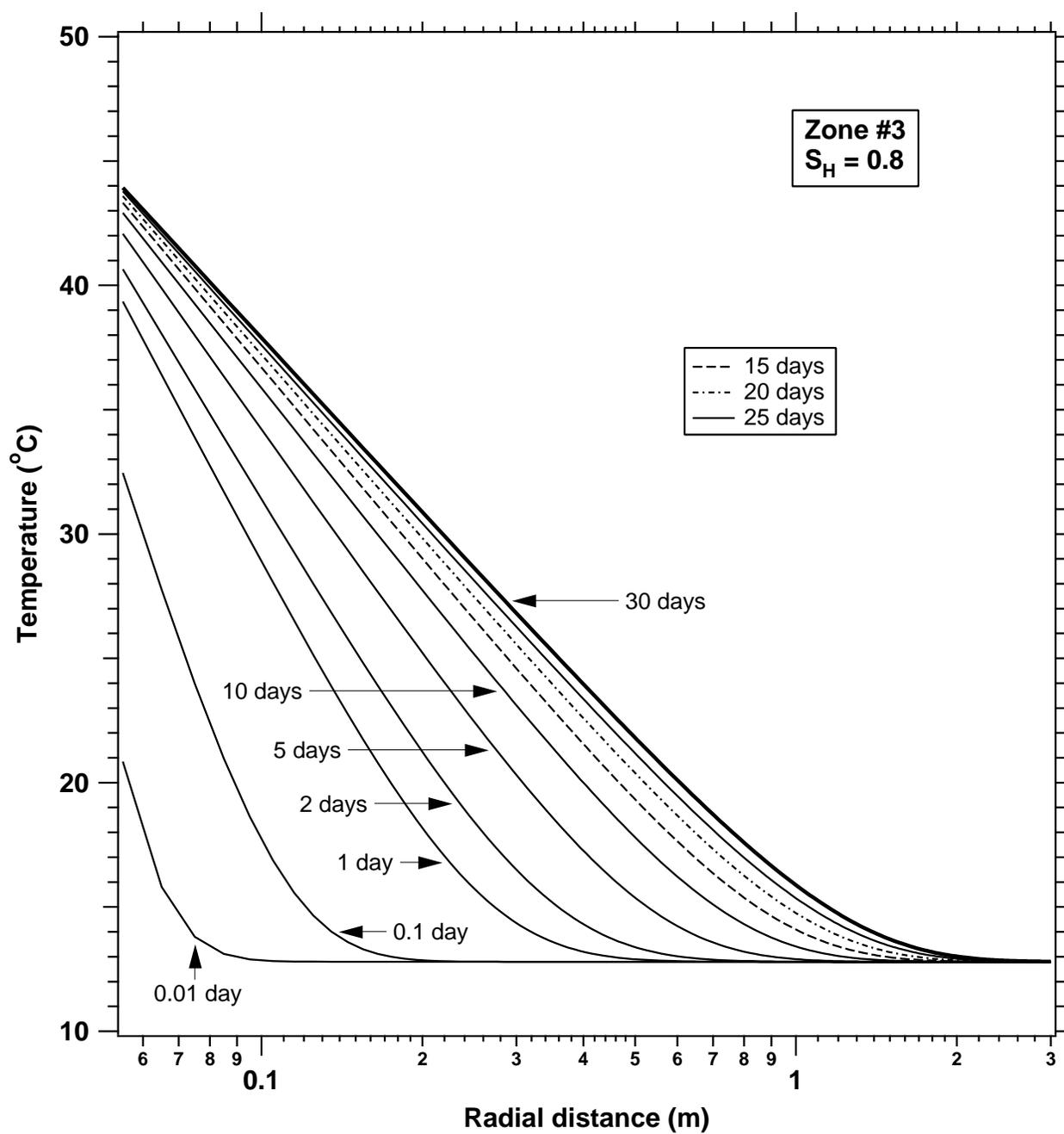
Fig. 11. Temperature distribution during thermal dissociation of hydrates in Zone #3.
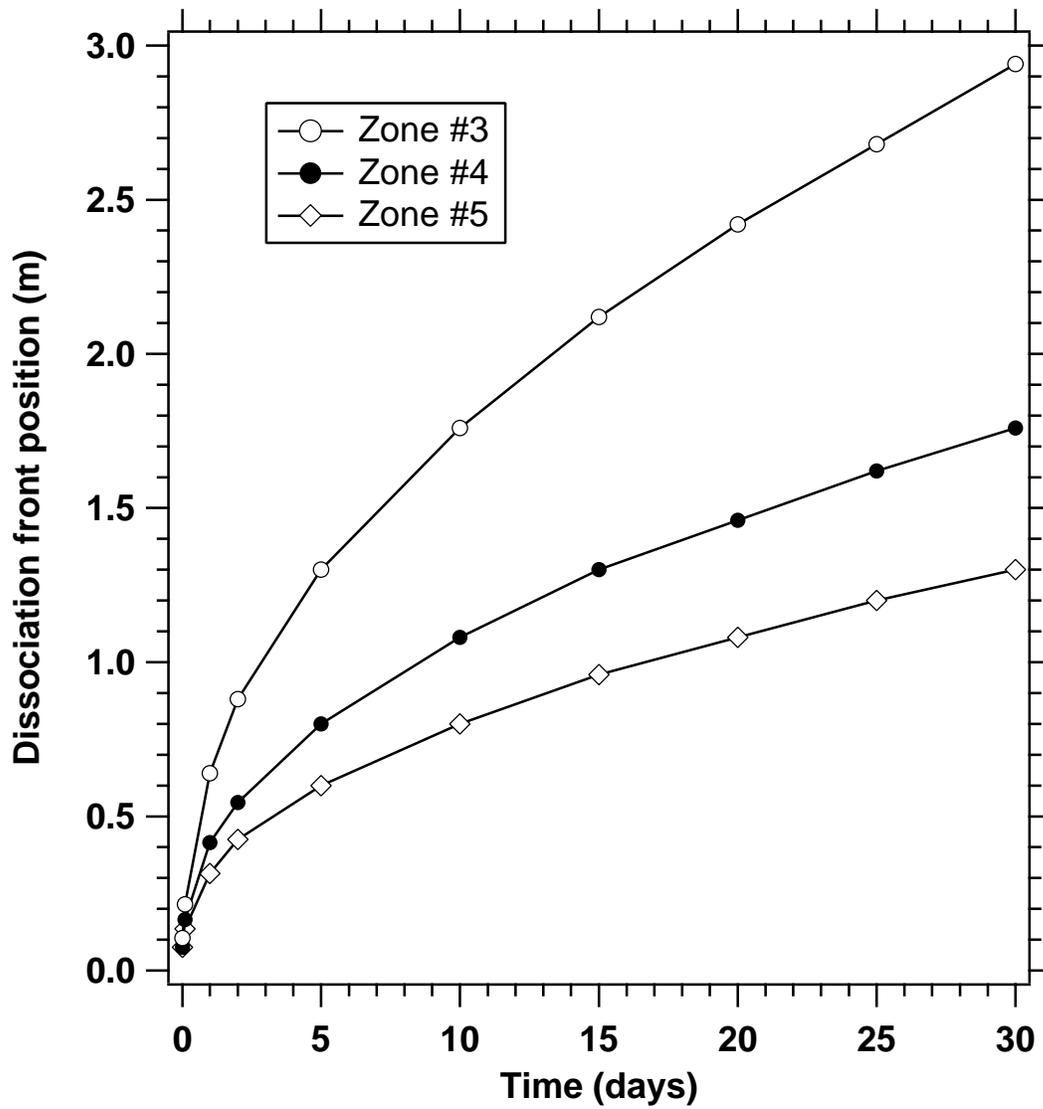
Fig. 12. Radii of the dissociation fronts in Zones #3 to #5.
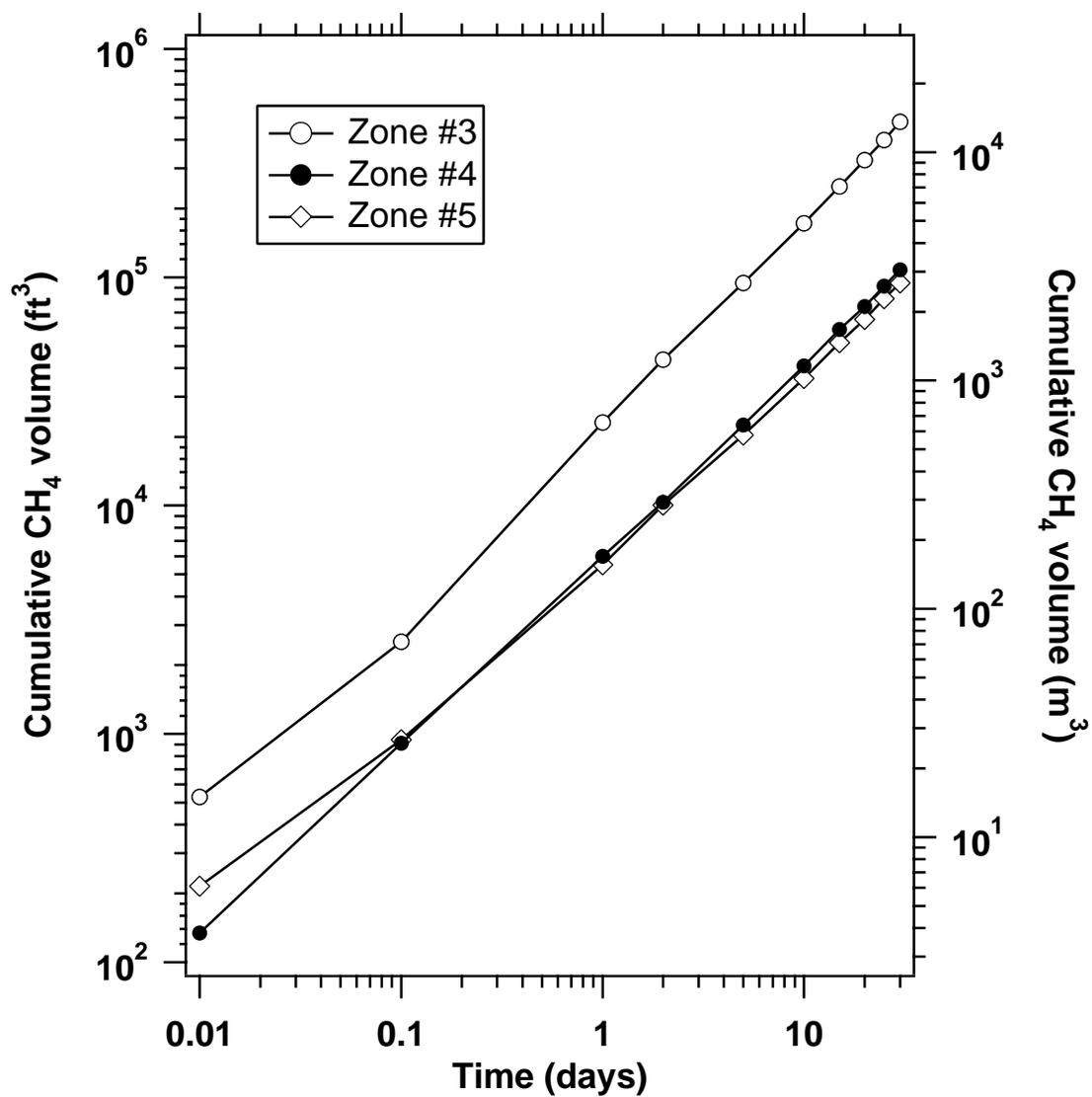
Fig. 13. Cumulative gas production in Zones #3, #4 and #5 (volumes in standard conditions).
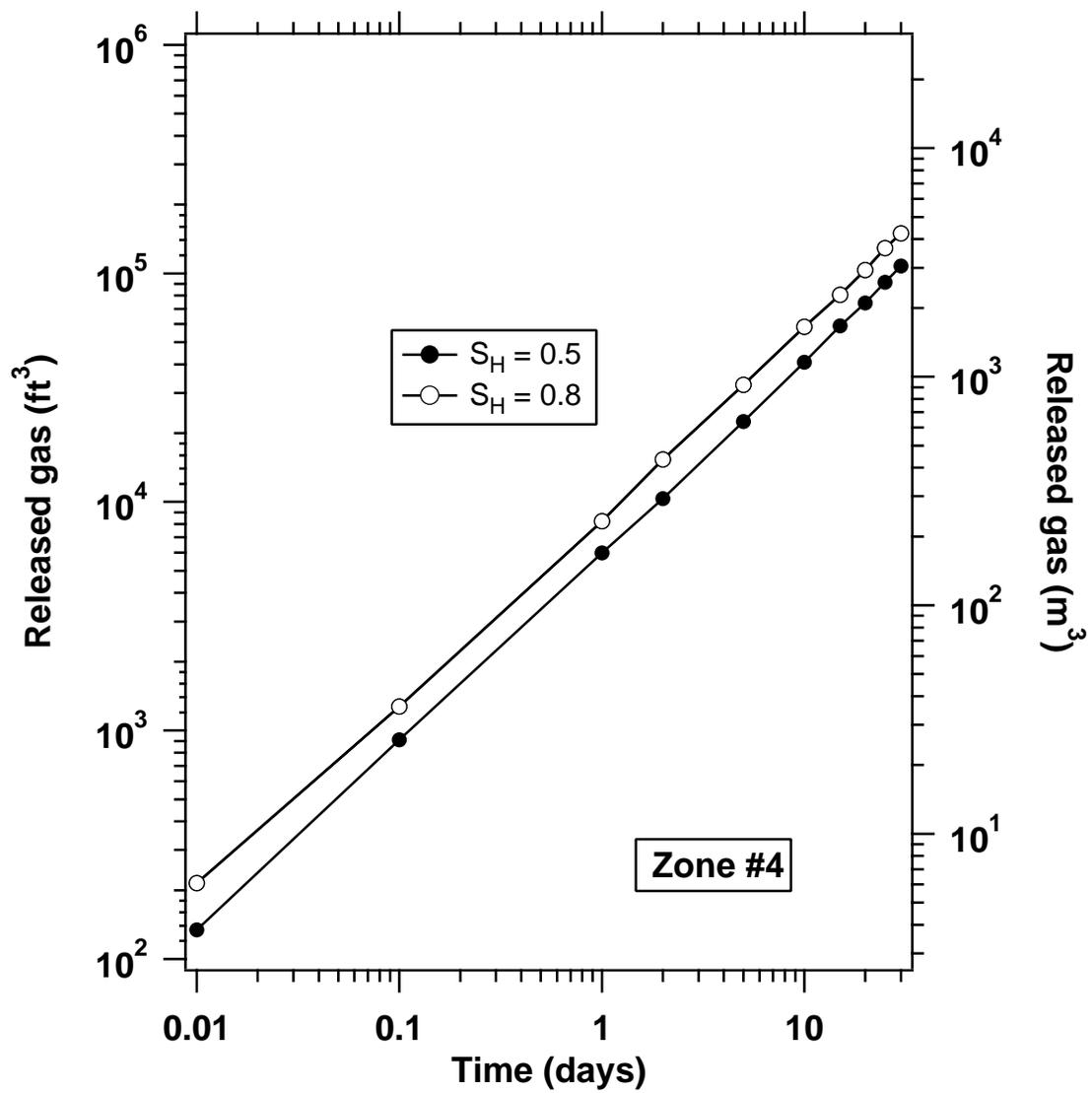
Fig. 14. Sensitivity of gas production to S_H in Zone #4 (volumes in standard conditions).
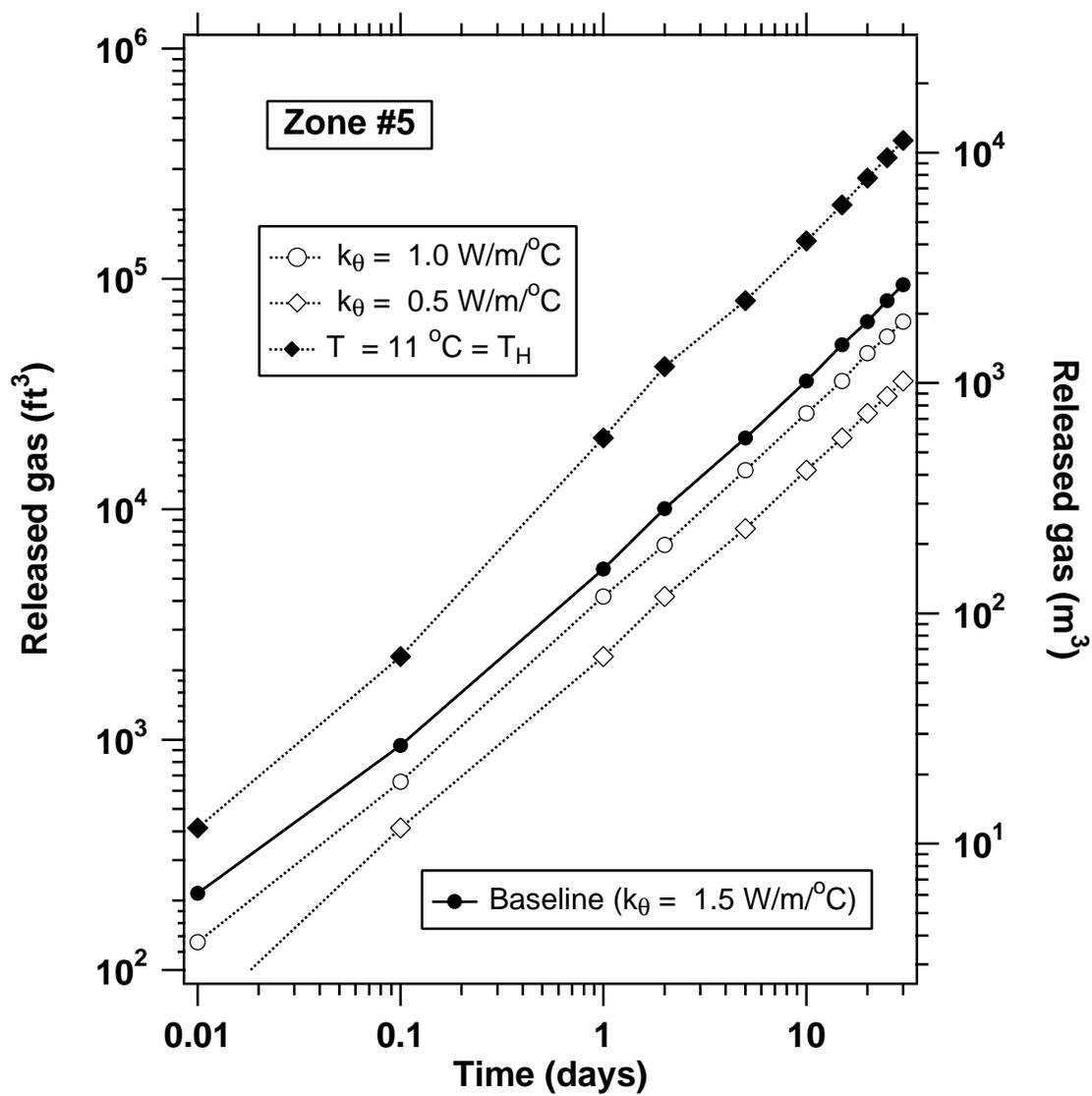
Fig. 15. Sensitivity of gas production to the thermal conductivity k_θ and to the hydrate initial temperature T.
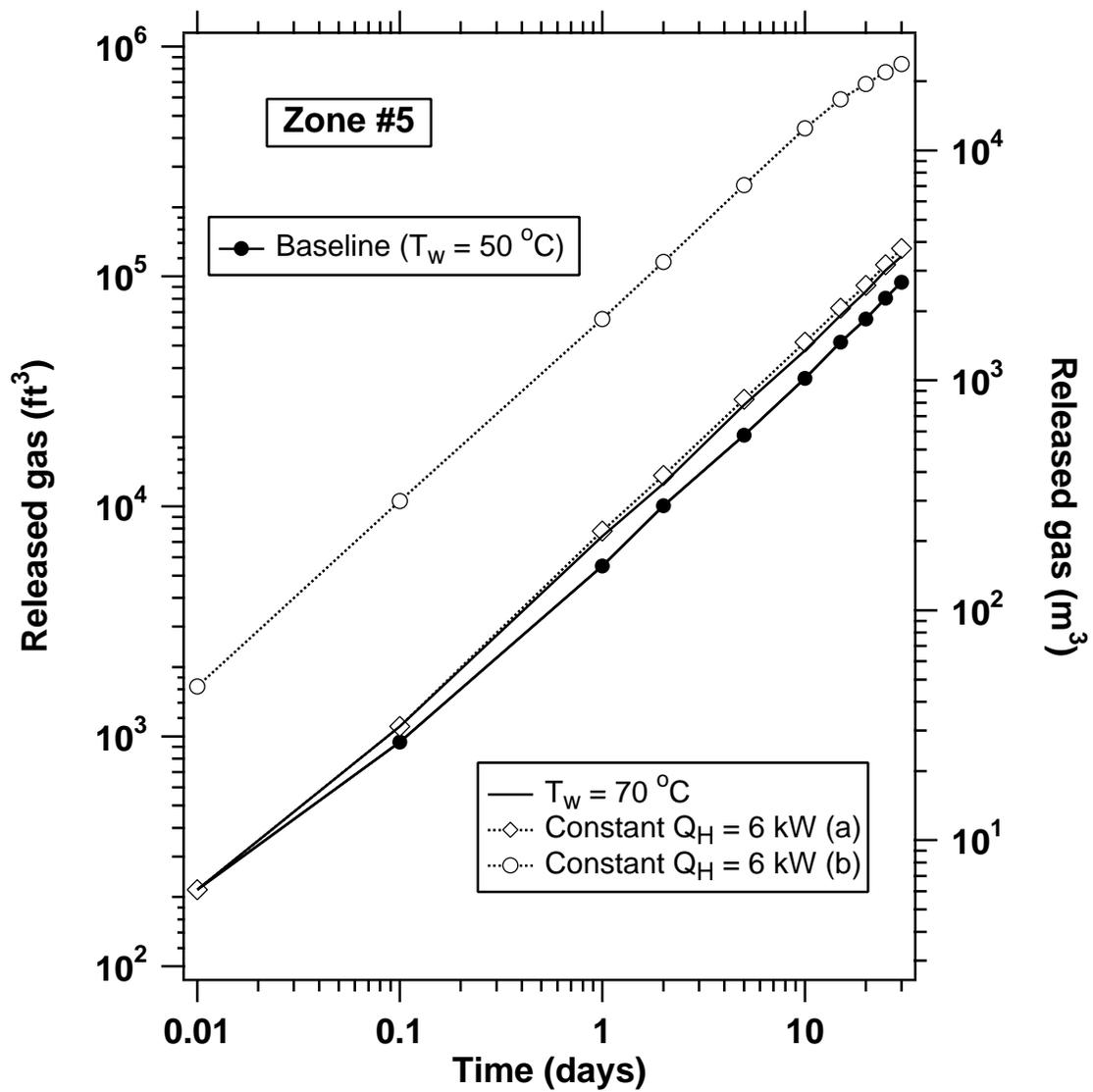
Fig. 16. Sensitivity of gas production to the method of heat addition and to the well boundary conditions.
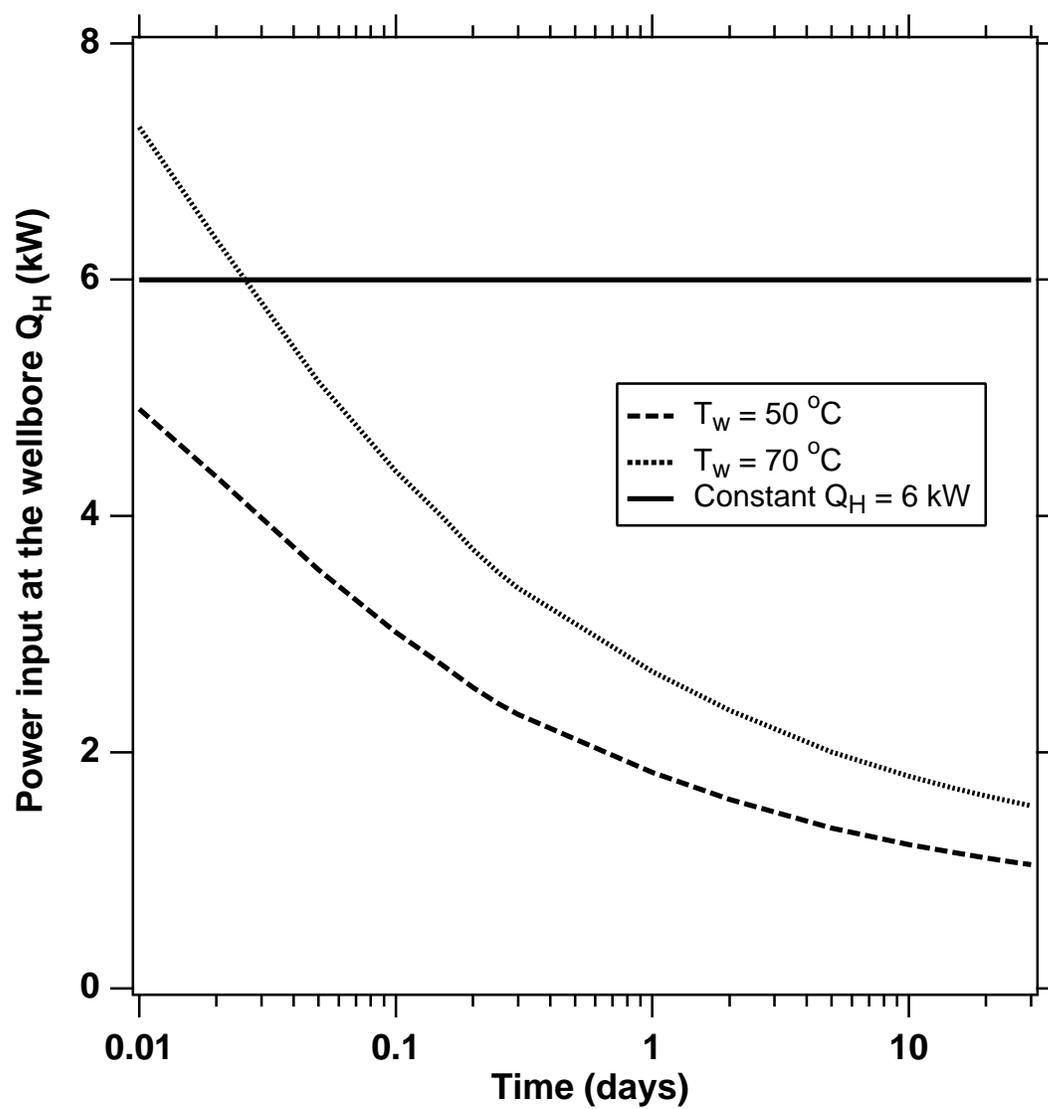
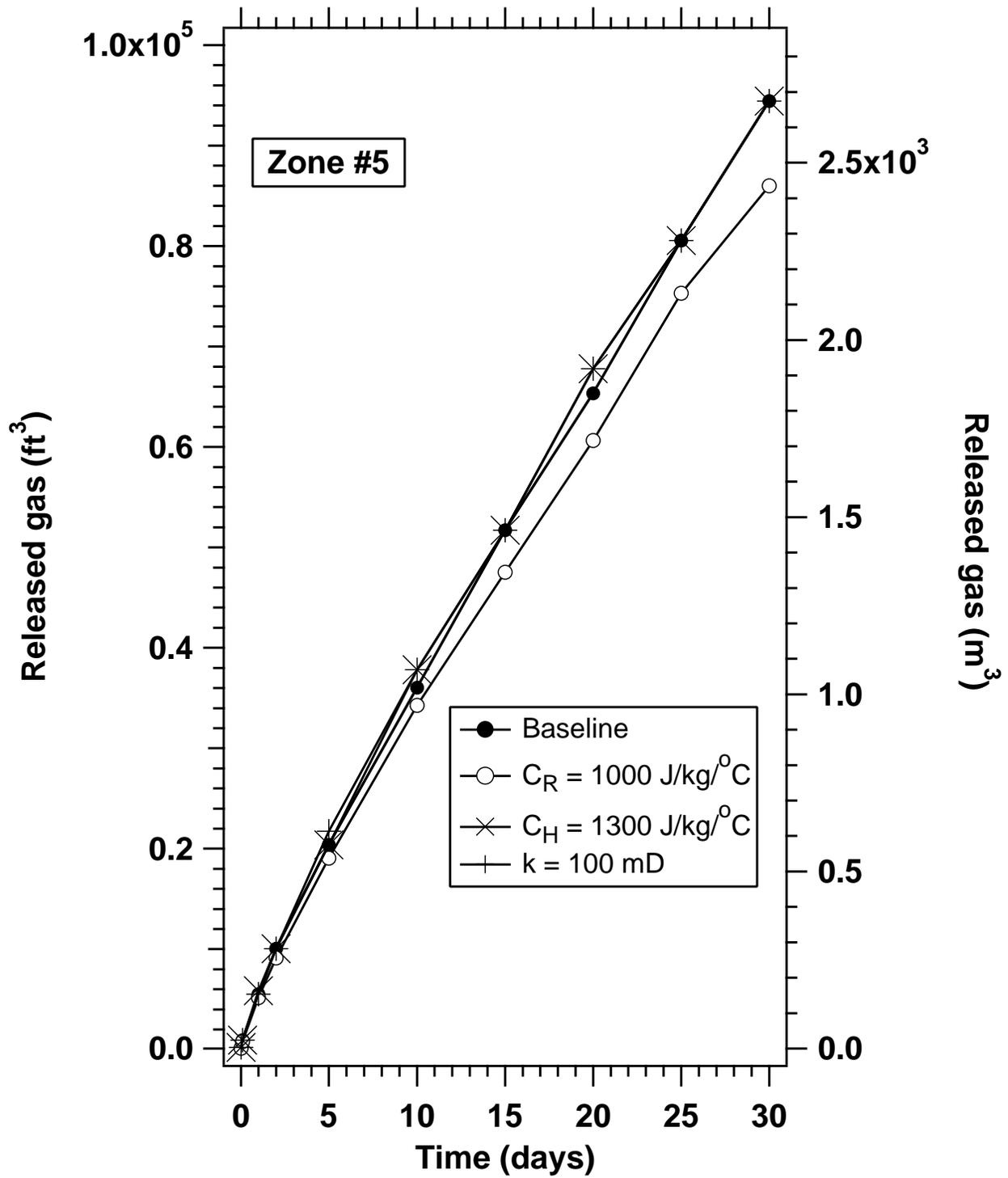Fig. 17. Power addition Q_H at the well for the different heating schemes.

Fig. 18. Sensitivity of gas production to the formation intrinsic permeability k, rock specific heat C_R and hydrate specific heat C_H.